ACS APPLIED MATERIALS & INTERFACES

www.acsami.org

Research Article

Effect of Solvents on a $Li_{10}GeP_2S_{12}$-Based Composite Electrolyte via Solution Method for Solid-State Battery Applications

Xinzhi Wang, Luhan Ye, Ce-Wen Nan, and Xin Li*

Cite This: https://doi.org/10.1021/acsami.2c12920

Read Online

ACCESS | Metrics & More | Article Recommendations | Supporting Information

ABSTRACT: Using a solution approach to process composite electrolytes for solid-state battery applications is a viable strategy for lowering the thickness of electrolyte layers and boosting the cell energy density. To fully utilize the super ionic conductivity of sulfides, more research about their solvent and binder compatibility is needed. Herein, the allowable solvent polarity is discovered through systematically pairing the solid electrolyte $Li_{10}GeP_2S_{12}$ (LGPS) with eight types of aprotic solvents. To further consider the influence of oxygen and moisture solvation that is important to practical manufacturing scenario, we also design experiments to flow dry air and N_2, or further mixed with water vapor, through these solvents to unveil their detrimental effects. Finally, a low polar solvent, dimethyl carbonate (DMC), and a previously unfavored commercial polymer, poly(vinylidene fluoride-*co*-hexafluoropropylene) (PVDF-HFP), are chosen to fabricate a ~40 μm thick LGPS-based composite electrolyte, giving 2 mS·cm^{-1} conductivity. It cycles between lithium/graphite composite electrodes at 0.5 mA·cm^{-2} for over 450 h with a capacity of 0.5 mAh·cm^{-2} and can withstand a 10-fold current surge.

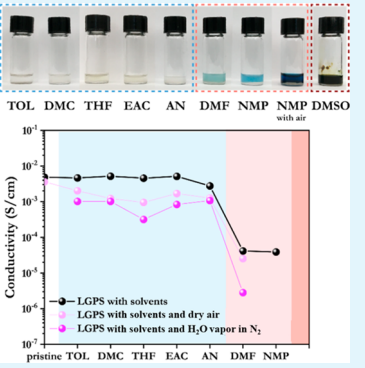

KEYWORDS: *solution approach, solvent effect, polymer binder, sulfide composite electrolyte, solid-state lithium-ion-battery*

INTRODUCTION

Lithium (Li)-ion battery based energy storage systems have been thrust into the spotlight by the market growth of electric automobiles, wearable devices, and renewable electricity.[1,2] In order to pursue the higher energy density and overcome the thermal peril, bulk-type inorganic all-solid-state lithium batteries with a Li anode (3860 mAh/g, 3.040 V vs standard hydrogen electrode theoretically) were constructed.[3−6] The problem of low ionic conductivity in many solid-state electrolytes was largely solved by the discovery of the sulfide family,[7] such as $Li_{10}GeP_2S_{12}$ (LGPS),[8] $Li_{9.54}Si_{1.74}P_{1.44}S_{11.7}Cl_{0.3}$ (LSPSCl),[9] and $70Li_2S{\cdot}30P_2S_5$[10] systems, whose conductivity can be comparable to liquid electrolytes. Making electrolyte powder directly into the bulk-type of electrolyte pellet, however, has to overcome certain technical challenges, including the high brittleness and thickness of the pellet that are detrimental to safety and energy density.[5,11−13] Despite the fact that techniques like sputtering, pulsed laser, and vapor-phase deposition can efficiently reduce thickness, they are not compatible with commercial mass production of batteries.[14−16] Polymer-inorganic composites are commonly regarded as a strategy for addressing the aforementioned difficulties.[17] The conductivity can be maintained, and the thickness can be controlled by slurry-casting below 100 μm.[18] The procedure is also compatible with commercial manufacturing platform for Li-ion batteries.

A typical method begins with a homogeneous precursor in solution or solid phase combining inorganic electrolyte granules and polymeric binders. The polymers can be poly(ethylene oxide) (PEO), polytetrafluoroethylene (PTFE), PVDF-HFP, and so on. It will be followed by slurry-casting and solvent evaporation or pressing with a hot calendaring machine. A polymer membrane could act as a skeleton in the process. Previously, Xu et al. and Xie et al. synthesized LGPS/PEO and LGPS/PVDF-HFP composite electrolytes, both with LGPS as the filler, and reported the maximum ionic conductivities of 1.18×10^{-5} and 1.8×10^{-4} S cm^{-1} at room temperature, respectively, which are substantially lower than that of the LGPS itself.[19,20] Bieker et al. examined the ionic conduction of LGPS/PEO with varied polymer compositions,[21] suggesting that unlike oxide solid electrolytes that simply serve as filler due to the low ionic conductivity, the sulfides tend to function as the conductive matrix in the composite, manifesting the higher ionic conductivity, while the polymer part becomes the filler instead.[22] To properly disperse the polymer filler in composite electrolytes, a solution method must be used, therefore selecting a proper solvent becomes important.

In past studies, researchers attempted to disperse sulfides in various solvents, including heptane, toluene (TOL), *p*-xylene, tetrahydrofuran (THF), acetonitrile (AN), *N*-methyl-2-pyrro-

Received: July 19, 2022
Accepted: September 27, 2022

lidone (NMP), and dimethylformamide (DMF).[23−25] It was found that exposure of sulfides to high polar aprotic solvents could cause a drastic drop in ionic conductivity; therefore, only nonpolar solvents could be used with sulfides. It is explained that when the polarity of the solvent increases, the solvation free energies of the decomposition products become more favorable.[24] The fact that sulfide composite electrolytes are restricted by low-polarity solvents is often misunderstood as only nonpolar polymers can be used. However, the maximum polarity of the solvents allowed in the LGPS system has yet to be determined. Moreover, in practice, solvents in large volumes always contain solvated oxygen and water. Their impact to a composite system has not been well understood.

In this work, we demonstrated a free-standing membrane formed by LGPS/PVDF-HFP composite electrolyte (LPCE) with a thickness of only 40 μm using the solution method, which allows the use of polar and more common binder, PVDF-HFP. With the addition of 5 wt % PVDF-HFP, the ionic conductivity reached 2 mS cm^{-1}. The influence of solvents and their solvated oxygen and vapor has been systematically studied. We find that the failure mechanism is attributed to the decomposition of sulfides in solvents with polarity beyond a certain limit. The solid-state symmetric batteries with the Li/graphite (Li/G) composite anode stably cycled for 450 h at 0.5 mA cm^{-2}. Also, these batteries can always return to normal cycling after a sharp current surge. Our work thus forms an important step toward understanding the right procedures of making a polymer ceramic composite electrolyte for the scaling-up application of solid state batteries based on sulfide electrolytes.

2. MATERIAL AND METHOD

2.1. Gas Treatment of LGPS Suspension. LGPS was obtained from Hefei Kejing Materials Technology Co., Ltd., or MSE Supplies and was not treated prior to usage. Various solvents, such as TOL (Sigma-Aldrich, 99.8%), DMC (Dodo Chem, H_2O < 100 ppm, 99%), THF (Dodo Chem, H_2O < 100 ppm, 99%), ethyl acetate (EAC, Sigma-Aldrich, 99.8%), AN (Sigma-Aldrich, 99.8%), DMF (Dodo Chem, H_2O < 100 ppm, 99%), NMP (Dodo Chem, H_2O < 100 ppm, 99%), or dimethyl sulfoxide (DMSO, Dodo Chem, H_2O < 100 ppm, 99%) were added into LGPS powder in Ar-filled glovebox ([H_2O] < 0.1 ppm, [O_2] < 0.1 ppm) at a concentration of 10 mg/mL. In fume hood, 10 mL of suspension was immediately transferred into a gas-washing bottle and exposed to artificial air or N_2 with saturated water vapor (∼1 vol %) with a total flow rate of 15 mL/min (calibrated at 25 °C) controlled by gas flow station.

2.2. LPCE Synthesis. PVDF-HFP (M_w ∼ 700,000, Arkema) powder was dissolved in DMC, stirring at 55 °C for 15 min with concentrations ranging from 40 to 120 mg/mL. The various concentrations depend on the expected amount of polymer in the composite slurry. The viscosity was kept under control to fully dissolve polymer and evenly blend LGPS. A gluelike polymer solution with appropriate viscosity was applied to various weights of LGPS powder to fabricate a thin film with the polymer weight ratios ranging from 2.5 to 45% (hereafter labeled as LPCE-2.5 or LPCE-40, with the number representing the weight ratio of polymer). It was stirred at 55 °C for only 15 min to avoid overevaporation, which allows a relatively precise regulation of the polymer amount by the solution volume. The slurry was then mixed before being coated on a 12 mm diameter stainless-steel (SS) electrode. Finally, the dried LPCE was pressed under 200 MPa in a homemade mold and then peeled off.

2.3. Material Characterization. After solvent immersion, the LGPS powder was dried in the vacuum chamber of glovebox. All samples were carefully sealed between characterizations and then transferred to a vacuum environment as quickly as possible. Scanning electron microscopy (SEM, Zeiss Merlin compact) was used to examine the morphology. X-ray photoelectron spectroscopy (XPS, PHI Quantera II, Ulvac-Phi) was utilized to detect surface chemistry with a monochromatic Al Kα X-ray source. The Ar source was used for depth profiling analysis, and the overall sputtering time was 54 s, corresponding to a etching rate of 0.185 nm/s on SiO_2. X-ray diffraction (XRD, Empyrean) at 40 kV and 40 mA with a Cu Kα radiation source was used for phase identification with a scanning rate of 5°/min. To avoid air contamination during the XRD test, the samples were sealed with a polyimide membrane (5um). Raman spectroscopy (LabRAM HR Evolution, Horiba) was used at an excitation wavelength of 532 nm. The solution sample was sealed by an 8um quartz glass in a stainless-steel container to prevent oxidation. Ultraviolet visible absorption spectra (Shimadu-UV2600) was collected with centrifuged supernatant in quartz cuvettes.

2.4. Electrochemical Measurements. All electrochemical tests were conducted in homemade pressurized cells. After applying 200 MPa for 3 min using an automatic press (HY-12, Tianguang Instrument), the cell was fixed at 100 MPa. An impedance analyzer (IM6, Zahner-elecktrik) was used to assess ionic conductivity in SS|LPCE|SS symmetric cells across a frequency range from 0.1 Hz to 8 MHz (amplitude 10 mV). The ionic conductivity (σ), was calculated using the formula $\sigma = L/[(R_1 + R_2)\cdot S]$, where L and S are the thickness and area of the electrolyte membrane, respectively. The equivalent circuit in Figure 5b is modeled and fit by R_1 as the bulk impedance, R_2 as the interface impedance, constant-phase element (CPE) as the interface capacitance, and W_o as the Warburg impedance that mimics ion diffusion behavior. Li/G composite serves as a lithium source as we previously reported.[26] Graphite forms a thin layer when combined with PTFE at a weight ratio of 95:5. We use 10 mm diameter Li foil and 12 mm diameter graphite foil. Linear sweep voltammetry (LSV) was carried out on the electrochemical workstation (Bio-Logic SAS, VMP3) using a Li/G|LPCE|SS cell at a scan rate of 0.1 mV·s^{-1}. Li/G|LPCE|Li/G cell was assembled to verify the cycling stability on a battery test system (C2001A, Land). All the tests were conducted at room temperature (∼25 °C).

3. RESULT AND DISCUSSION

3.1. Interaction between LGPS and Different Solvents. In this paper, we focus on the solution approach of composite fabrication, which is a method compatible with mass production of uniform film. We first evaluate solvent compatibility of LGPS, since it is the major matrix that contributes to the ionic conductivity. It was shown that solid sulfide electrolytes could be sensitive to moisture[27,28] and may decompose in water or protic solvent.[23] To test such a compatibility of LGPS, we selected various aprotic solvents with varying compositions and polarities, which were routinely applied in polymer composite fabrication.[19,20,29−31] The results are presented in Figure 1a, where 10 mg of LGPS was immersed in 1 mL of various ultrapure solvents and left still in a glovebox for 1 h. They can be classified into three types of reactions based on the intensity and color of the reacted

https://doi.org/10.1021/acsami.2c12920
ACS Appl. Mater. Interfaces XXXX, XXX, XXX−XXX

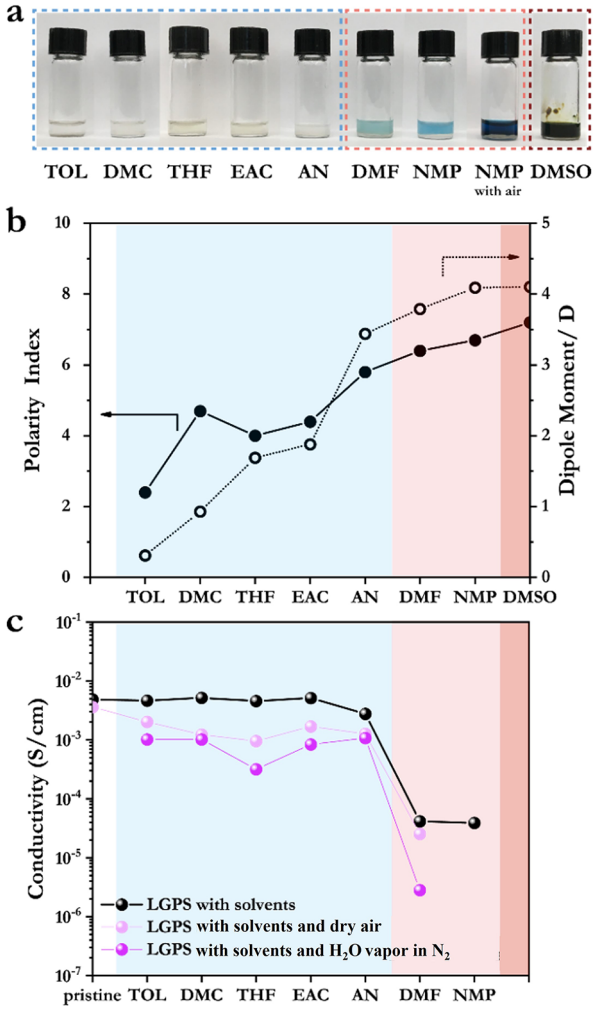

Figure 1. (a) Color difference of 10 mg of LGPS powder immersed in 1 mL of various solvents for 1 h. (b) Polarity index and dipole moment of corresponding solvents. (c) Ionic conductivity of LGPS measured after 1 h of dispersion in solvents and drying. The purple dots mark the powder conductivity after different gas treatment of the suspension. The blue, pink, and red frame or squares indicate different performance when LGPS is blended with solvents.

solution. First, in the boxed region by blue dashed lines in Figure 1a, the suspension was colorless or in very pale yellow mainly caused by LGPS itself. The pace of precipitation may also contribute to different color shades.[23] Second, in the pink boxed region in Figure 1a, the solvents were bright or dark blue, suggesting that a chemical reaction occurred, with the powder precipitation at the bottom maintaining its original color. We also accidently discovered that when the LGPS suspension in NMP was exposed to ambient air, it became darker, indicating that vapor or O_2 increased the color-changing reaction. Finally, in the dark red boxed region in Figure 1a, not only did the light yellow powder transformed vigorously into a dark green sticky substance but also there was a burst of gas release.

The polarity indices and dipole moments of the solvents are presented in Figure 1b.[25,32] According to their interactions with LGPS, low-polarity solvents cause slight dissolution, moderate-polarity solvents generate slight reaction, and high-polarity solvents cause severe reaction. Our observation here is thus consistent with an earlier computational study,[24] which shows that as the dielectric constant of solvents increases the decomposition reaction becomes energetically more favorable.

We further show that such decomposition reaction can cause a significant drop of the ionic conductivity (see Figure 1c, black dots, and Figure S1). After being immersed in several ultrapure solvents, filtered, and dried, 120 mg of LGPS powder was made into ∼550 μm thick pellets by 200 MPa external pressure and followed by an impedance measurement at 100 MPa. The conductivity only slightly decreases and remains at the same magnitude in the blue zone compared with the pristine one. However, it drops by 2 orders of magnitude when reaching the pink zone. This suggests that solvents in the pink region are already beyond the polarity limit that could be used with LGPS. We find that this limit also depends on the type of sulfide electrolytes, when comparing our LGPS measurement with $Li_7P_3S_{11}$,[24] Li_6PS_5Cl,[23] and $75Li_2S{\cdot}25P_2S_5$,[25,33] likely caused by different degradation reactions.

To mimic the possible contamination in raw solvent or during fabrication process, we also introduced either dry air or water vapor to the solvent. It shows that both had worse side effects and caused a decline in conductivity by one magnitude of order (see Figures 1c, purple dots, and S1). This suggests that both oxygen and H_2O could participate in the complicated reaction process with LGPS in solvents, further deteriorates the electrochemical property of LGPS.

3.2. LGPS Reaction with Low-Polarity Solvents. To better understand the decomposition process, XRD, XPS, and Raman spectra were performed to study the reacted LGPS following the immersion and drying process, as well as the supernatant after centrifugation.

As seen in Figure 2a–c, the amorphous phase was only found with DMSO, which lost all characteristic peaks of LGPS. All other processed LGPS preserved its original XRD pattern. This suggests that most color-changing reactions may have only happened on a thin surface layer of the LGPS particles, without changing the main crystalline phase of remaining LGPS.

The binding energies of the collected LGPS powder after reactions were also measured. The Li 1s and P 2p spectra were unchanged across all solvents (Figure 2d,e). However, with DMF and NMP, the peak profiles of Ge 3d were blue-shifted, indicating an oxidization of Ge, while the S 2p peaks displayed an extra peak at 167.3 eV that represents certain sulfur product with higher valence than −2 (Figure 2f,g). The relatively lower peak intensity further verified the Ge and S consumption. In Figure 2f,g, a depth profile was also performed to better understand the microstructure of the obtained LGPS following this solvent-induced degradation. Note that 10 nm of the SiO_2 reference sample was sputtered away. Since SiO_2 (∼36 GPa) shows a bulk modulus similar to that of LGPS (∼30 GPa),[34,35] we estimate that they should show similar Ar^+ etching speed following a previous argument;[36] thus, the depth of this residue layer from decomposition reaction is estimated to be around 10 nm.

With both medium-polarity DMF and NMP, the LGPS solution had a vivid blue color (Figure 1a). In Raman spectra, the characteristic symmetric stretching vibration of $[S_3]^{\bullet-}$ was observed at 535 cm^{-1}, accompanied by a series of overtone progressions observed at 1070 and 1605 cm^{-1} (Figure 3a,c).[37] An absorption maximum at 617 nm in the UV–visible has also been detected as Figure 3b,d, which confirms the existence of $[S_3]^{\bullet-}$.[37,38] The decomposition component of $[S_3]^{\bullet-}$ suggests that LGPS surface deterioration was caused by certain

https://doi.org/10.1021/acsami.2c12920
ACS Appl. Mater. Interfaces XXXX, XXX, XXX−XXX

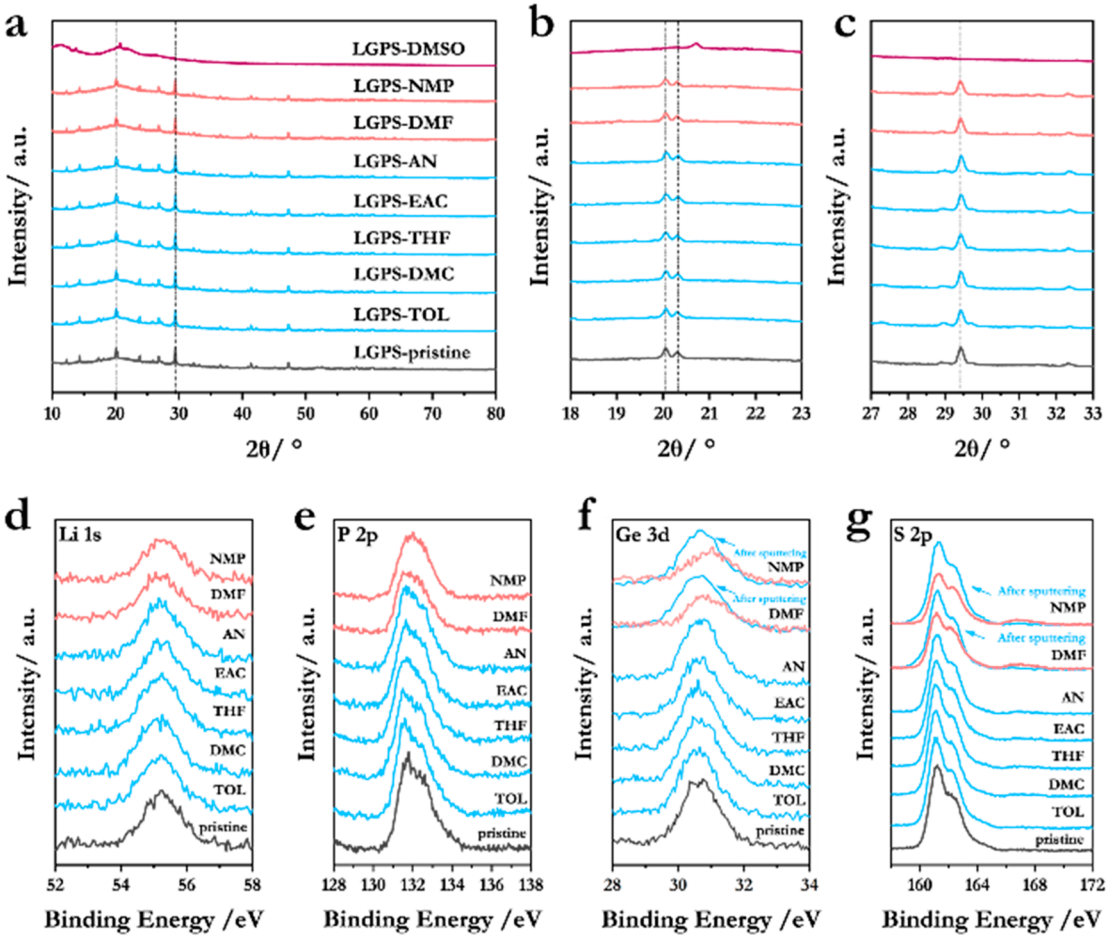

Figure 2. (a–c) XRD pattern of dried LGPS powder after dispersion in solvents (a) and the enlarged peak pattern at 20.1° (b) and 29.4° (c). (d–g) XPS spectra of Li 1s (d), P 2p (e), Ge 3d (f), and S 2p (g) regions showing the combined binding energies of collected LGPS powder after dispersion. Depth profiles are marked with blue arrow.

common LGPS oxidation reaction. The suspension kept the original spectra and showed no color change while using low-polarity solvents such as THF (Figure S2).

3.3. Solvated Moisture and Air. We consider the capability of a material to maintain its original composition, phase, and functions while exposed to air as the air stability.[39] This is a crucial aspect of solid electrolyte especially in large-scale manufacturing.[40] The final conductivity could be greatly influenced by the solvated oxygen in purchased solvents and from the ambient during casting and evaporation.[41] To compare the sensitivity of LGPS with low-polarity DMC and moderate-polarity NMP and understand the respective mechanisms of air and moisture, an experiment was designed by flowing artificial dry air with ~21 vol % O_2 or N_2 or further mixed with saturated water vapor, through gas-washing bottles holding either suspension or supernatant.

The LGPS suspension with DMC basically remained the same color after 2 min continuous contact with dry air (Figure S3a) or moisture (Figure S4a). When the blue NMP supernatant was exposed to dry air, it turned yellow (Figure S3b), indicating that the $[S_3]^{\bullet-}$ was oxidized to $[S_4]^{\bullet-}$ or other polysulfide's anions.[37] The color of blue LGPS suspension darkened after being exposed to dry air, implying that O_2 likely has aided this reaction for a color change to blue (Figure S3c). When infused with water vapor for 2 min, the NMP supernatant (Figure S4b) and suspension (Figure S4c) of LGPS in NMP maintained its bright blue color. We dropped 2 mL of water in the two cases to distinguish their responses. The supernatant stayed unchanged, while the color of the suspension faded with odor release and visible powder consumption, which should come from the sulfide powder reacting directly with water.[42]

To summarize, we used gas flow experiments to isolate the effects of O_2 and H_2O, and we discovered that it was O_2 that caused LGPS degradation, generating the unique blue color from $[S_3]^{\bullet-}$. Water vapor also caused LGPS decay and odor release, though enough amount of water was needed. Low-polarity solvents could prevent these negative effects to some degree while preserving LGPS's high conductivity. Thus, low oxygen and humidity environments are not only essential in stirring, casting, and evaporation processes but also the solvated O_2 and H_2O in raw solvents and during their storage should be avoided.

3.4. Structure and Electrical Properties of LPCE. LPCE membranes were prepared by mixing the LGPS powder with a PVDF-HFP precursor in DMC with low polarity, then casting and evaporating the solvent. We selected DMC as the solvent not only because of its low harm to LGPS conductivity but also for its environmental friendliness that was proposed as a green solvent.[43] The LGPS powder with particle size of 1–5 μm was used as purchased and characterized by SEM (Figure 4a). LPCEs with varied polymer weight ratios were fabricated in

https://doi.org/10.1021/acsami.2c12920
ACS Appl. Mater. Interfaces XXXX, XXX, XXX–XXX

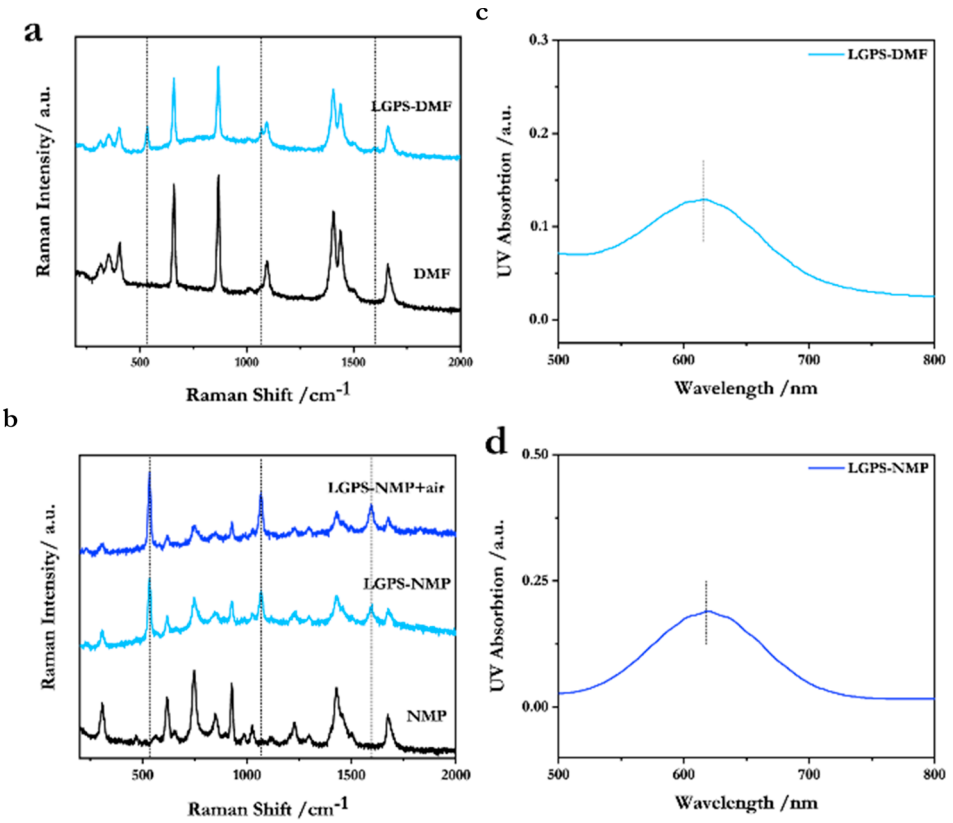

Figure 3. Raman spectra of the supernatant DMF(a) and NMP(b) solution with LGPS. The UV−visible absorption spectra of the supernatant DMF(c) and NMP(d) solution with LGPS.

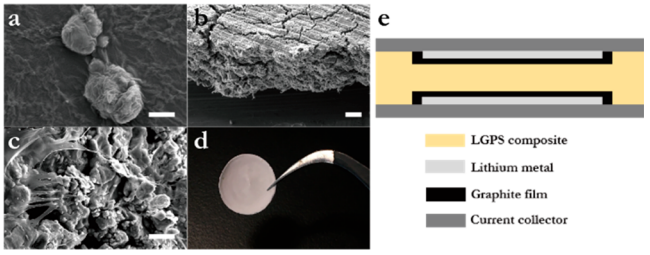

Figure 4. SEM image of pristine LGPS particles (a, scale bar = 2 μm), cross-sectional view (b, scale bar = 10 μm), and top view (c, scale bar = 10 μm) of LPCE-5. (d) Optical image of a LPCE-5 with a diameter of 12 cm. (e) Configuration illustration of Li/G+LPCE symmetrical cell assembly.

roughly 40 μm thickness, which is comparable to the thickness of commercial separator. Figures 4b−d show the homogeneous microview and self-standing macroview of LPCE-5. Some polymer filaments were seen in the top view showing satisfactory adherence.

The cell was made by stacking the Li/G electrode film and the LPCE layer together (Figure 4e). In light of the instability between Li foil and LGPS, a protective graphite coating has been developed as we previously reported.[26] The cell was maintained at 100 MPa operational stack pressure during all the battery tests below, after a mechanical molding at 200 MPa. This mechanically constricted cell test condition can help both improve electrochemical stability and maintain excellent interface contact.[44,45]

The Nyquist plots (Figure 5a) of LPCE-based symmetric cell fit well into two parts, a suppressed semicircle at middle−high frequency and a linear section at low frequency. The interface impedance, which can be represented by an equivalent circuit of parallel-connected resistor and capacitor, gives the semicircle. The line tail is attributed to the carrier transport when compared to a Warburg resistor.[46] As shown in Figure 5a, when polymer ratios rose from 5 to 20 wt %, both bulk and interface impedance increased, indicating that the polymer offered film formability at the expense of ionic conductivity, particularly at the interface, as seen by the considerably larger semicircles. This increased contact impedance will reduce the total ionic conductivity. The ionic conductivity values were listed in Figure 5b. LPCE-2.5 had the longest error bar because of uneven distribution during sample preparation. It was also exceedingly brittle and could not stand alone when being peeled off from the electrode. Therefore, LPCE-5 with an ionic conductivity of ∼2 mS cm^{-1} and areal conductance of ∼500 mS cm^{-2} is the best composite composition that could be reliably fabricated here.

The LSV test was used to determine the electrochemical stability of LPCE (Figure 5c). Below 5.5 V, no noticeable breakdown occurred, making it appropriate for most high-voltage cathode materials. Li stripping and plating were repeated using Li/G|LPCE-5|Li/G cell for 1 h of charging and discharging at 25 °C with a current density of 0.5 mA·cm^{-2}. The polarization voltage in constant current galvanostatic cycle was as low as 0.2 V and stable for 450 h (Figure 5d). The reduction in overpotential at the start of cycling might be explained by better contact between the LPCE and Li/G composite electrode, as well as the integration of Li/G composite.[26] A battery test was designed as shown in Figure 5e to further examine the cycling performance of LPCE at a higher rate. It started at 0.2 mA·cm^{-2} for 5 cycles before

https://doi.org/10.1021/acsami.2c12920
ACS Appl. Mater. Interfaces XXXX, XXX, XXX−XXX

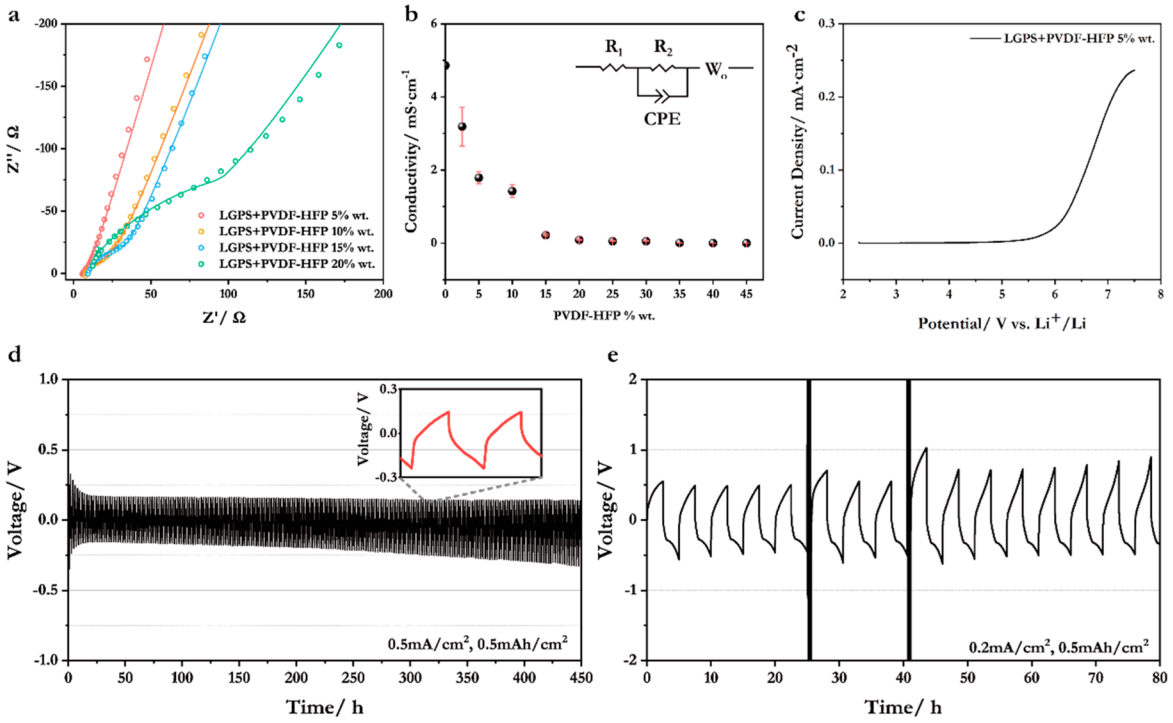

Figure 5. Nyquist plots (a) and ionic conductivity (b) of the LPCEs with different amounts of PVDF-HFP. The inset shows the equivalent circuit. (c) LSV plot of the LPCE-5. (d) Li plating and stripping at 0.5 mA·cm^{-2} and 0.5 mAh·cm^{-2} per cycle across LPCE with an enlarged cycle profile inserted. (e) After voltage spikes induced by high current density of 5 or 10 mA·cm^{-2}, the battery can always be recovered when the current density is set back to 0.2 mA·cm^{-2}.

jumping to 5 mA·cm^{-2} charging, resulting in a strong voltage spike and a safety stop at 5 V for 5 times. It was then reset to 0.2 mA·cm^{-2} for 3 cycles before being increased to 10 mA·cm^{-2} with another safety stop. However, with a slightly greater overpotential, the cell was always able to cycle at 0.2 mA·cm^{-2} again. Based on the aforementioned characterizations and understandings of LPCEs, further development of technologies based the composite electrolyte strategy provides a promising pathway for the scaling-up application of solid-state batteries.

4. CONCLUSIONS

In conclusion, we adopted a solution approach to process LGPS-based composite electrolyte and emphasize the criteria for selecting solvents in our research. LGPS shows three scenarios in contact with aprotic solvents: minor dissolution in TOL, DMC, THF, EAC, and AN, mild reaction in DMF and NMP, and severe reaction in DMSO, which is highly correlated with solvent's polarity. In LGPS, the major breakdown is related to Ge and S. $[S_3]^{\bullet-}$ has been recognized as the typical blue substance in the reacted solution. Short-term exposure to low-polarity solvents has no discernible effect on conductivity. Solvated oxygen and moisture, which could be introduced from the raw solvents or the casing and evaporation processes, causes noticeable degradation, especially in high-polarity solvents. We systematically studied this phenomenon through experiments with LGPS and solvents being flown through by dry air or N_2 with water vapor, which shows that the low-polarity solvents can also effectively inhibit the side effects. We finally use ultrapure DMC as the solvent and keep the atmosphere under strict control. We present a composite electrolyte with 95 wt % LGPS to balance film formability and ionic conductivity. It shows an ionic conductivity of 2 mS·cm^{-1} and can maintain a voltage stability window of up to 5.5 V. When sandwiched between Li/G electrodes, the cell can cycle at 0.5 mA·cm^{-2} for over 450 h with a capacity of 0.5 mAh·cm^{-2} and recover without obvious overpotential even after repeated high-current surges. The polarity limit identified in this study, as well as the experimental methodology involving solvated oxygen and moisture, may help new material selection and design in the future, which might lead to more scalable technologies for high-performance, low-cost, solid-state batteries.

■ ASSOCIATED CONTENT

Supporting Information

The Supporting Information is available free of charge at https://pubs.acs.org/doi/10.1021/acsami.2c12920.

Nyquist plots of the LPCE with different amounts of PVDF-HFP, Raman spectra of the supernatant THF solution with LGPS, screenshots of artificial air and saturated water vapor pouring in LGPS suspension or supernatant (PDF)

■ AUTHOR INFORMATION

Corresponding Author

Xin Li − *John A. Paulson School of Engineering and Applied Sciences, Harvard University, Cambridge, Massachusetts 02138, United States;* orcid.org/0000-0001-9390-0830; Email: lixin@seas.harvard.edu

Authors

Xinzhi Wang − *John A. Paulson School of Engineering and Applied Sciences, Harvard University, Cambridge, Massachusetts 02138, United States; School of Materials Science and Engineering, Tsinghua University, Beijing 100084, China*

https://doi.org/10.1021/acsami.2c12920
ACS Appl. Mater. Interfaces XXXX, XXX, XXX−XXX

Luhan Ye − *John A. Paulson School of Engineering and Applied Sciences, Harvard University, Cambridge, Massachusetts 02138, United States;* orcid.org/0000-0002-2684-424X

Ce-Wen Nan − *School of Materials Science and Engineering, Tsinghua University, Beijing 100084, China*

Complete contact information is available at: https://pubs.acs.org/10.1021/acsami.2c12920

Notes

The authors declare no competing financial interest.

■ ACKNOWLEDGMENTS

The work performed at Harvard University was supported by Harvard Climate Change Solutions Fund and partly supported by the Assistant Secretary for Energy Efficiency and Renewable Energy (EERE), Vehicle Technology Office (VTO), of the U.S. Department of Energy (DOE) through the Advanced Battery Materials Research (BMR) Program. X.W. thanks the China Scholarship Council (CSC) for support as a visiting scholar at Harvard. Partial experiments performed at Tsinghua was supported by the Basic Science Center Program of National Natural Science Foundation of China (NSFC).

■ REFERENCES

(1) Tarascon, J. M.; Armand, M. Issues and Challenges Facing Rechargeable Lithium Batteries. *Mater. Sustainable Energy* **2011**, 171−179.

(2) Liu, J.; Bao, Z.; Cui, Y.; Dufek, E. J.; Goodenough, J. B.; Khalifah, P.; Li, Q.; Liaw, B. Y.; Liu, P.; Manthiram, A.; et al. Pathways for Practical High-Energy Long-Cycling Lithium Metal Batteries. *Nat. Energy* **2019**, *4* (3), 180−186.

(3) Goodenough, J. B.; Kim, Y. Challenges for Rechargeable Li Batteries. *Chem. Mater.* **2010**, *22* (3), 587−603.

(4) Choi, N. S.; Chen, Z.; Freunberger, S. A.; Ji, X.; Sun, Y. K.; Amine, K.; Yushin, G.; Nazar, L. F.; Cho, J.; Bruce, P. G. Challenges Facing Lithium Batteries and Electrical Double-Layer Capacitors. *Angew. Chem., Int. Ed.* **2012**, *51* (40), 9994−10024.

(5) Niu, C.; Liu, D.; Lochala, J. A.; Anderson, C. S.; Cao, X.; Gross, M. E.; Xu, W.; Zhang, J. G.; Whittingham, M. S.; Xiao, J.; Liu, J. Balancing Interfacial Reactions to Achieve Long Cycle Life in High-Energy Lithium Metal Batteries. *Nature Energy* **2021**, *6* (7), 723−732.

(6) Cheng, X. B.; Zhao, C. Z.; Yao, Y. X.; Liu, H.; Zhang, Q. Recent Advances in Energy Chemistry between Solid-State Electrolyte and Safe Lithium-Metal Anodes. *Chem.* **2019**, *5* (1), 74−96.

(7) Wu, J.; Liu, S.; Han, F.; Yao, X.; Wang, C. Lithium/Sulfide All-Solid-State Batteries Using Sulfide Electrolytes. *Adv. Mater.* **2021**, *33* (6), 2000751.

(8) Kamaya, N.; Homma, K.; Yamakawa, Y.; Hirayama, M.; Kanno, R.; Yonemura, M.; Kamiyama, T.; Kato, Y.; Hama, S.; Kawamoto, K.; Mitsui, A. A Lithium Superionic Conductor. *Nat. Mater.* **2011**, *10* (9), 682−686.

(9) Kato, Y.; Hori, S.; Saito, T.; Suzuki, K.; Hirayama, M.; Mitsui, A.; Yonemura, M.; Iba, H.; Kanno, R. High-Power All-Solid-State Batteries Using Sulfide Superionic Conductors. *Nat. Energy* **2016**, *1* (4), 16030.

(10) Seino, Y.; Ota, T.; Takada, K.; Hayashi, A.; Tatsumisago, M. A Sulphide Lithium Super Ion Conductor is Superior to Liquid Ion Conductors for Use in Rechargeable Batteries. *Energy Environ. Sci.* **2014**, *7* (2), 627−631.

(11) Wan, H.; Liu, S.; Deng, T.; Xu, J.; Zhang, J.; He, X.; Ji, X.; Yao, X.; Wang, C. Bifunctional Interphase-Enabled $Li_{10}GeP_2S_{12}$ Electrolytes for Lithium−Sulfur Battery. *ACS Energy Letters* **2021**, *6* (3), 862−868.

(12) Yu, X.; Manthiram, A. Electrode−Electrolyte Interfaces in Lithium−Sulfur Batteries with Liquid or Inorganic Solid Electrolytes. *Accounts of chemical research* **2017**, *50* (11), 2653−2660.

(13) Kobayashi, T.; Inada, T.; Sonoyama, N.; Yamada, A.; Kanno, R. All Solid-State Batteries Using Super Ionic Conductor. *MRS Proc.* **2004**, *835*, K11.1.

(14) Wang, Y.; Liu, Z.; Zhu, X.; Tang, Y.; Huang, F. Highly Lithium-Ion Conductive Thio-LISICON Thin Film Processed by Low-Temperature Solution Method. *J. Power Sources* **2013**, *224*, 225−229.

(15) Sakuda, A.; Hayashi, A.; Ohtomo, T.; Hama, S.; Tatsumisago, M. All-Solid-State Lithium Secondary Batteries Using $LiCoO_2$ Particles with Pulsed Laser Deposition Coatings of $Li_2S−P_2S5$ Solid Electrolytes. *J. Power Sources* **2011**, *196* (16), 6735−6741.

(16) Ogawa, M.; Kanda, R.; Yoshida, K.; Uemura, T.; Harada, K. High-Capacity Thin Film Lithium Batteries with Sulfide Solid Electrolytes. *J. Power Sources* **2012**, *205*, 487−490.

(17) Fan, L. Z.; He, H.; Nan, C. W. Tailoring Inorganic−Polymer Composites for the Mass Production of Solid-State Batteries. *Nat. Rev. Materials* **2021**, *6*, 1003−1019.

(18) Xiao, Z.; Long, T.; Song, L.; Zheng, Y.; Wang, C. Research Progress of Polymer-Inorganic Filler Solid Composite Electrolyte for Lithium-Ion Batteries. *Ionics* **2021**, *28*, 15−26.

(19) Cong, L.; Li, Y.; Lu, W.; Jie, J.; Liu, Y.; Sun, L.; Xie, H. Unlocking the Poly (vinylidene fluoride-co-hexafluoropropylene)/$Li_{10}GeP_2S_{12}$ Composite Solid-State Electrolytes for Dendrite-Free Li Metal Batteries Assisting with Perfluoropolyethers as Bifunctional Adjuvant. *J. Power Sources* **2020**, *446*, 227365.

(20) Zhao, Y.; Wu, C.; Peng, G.; Chen, X.; Yao, X.; Bai, Y.; Wu, F.; Chen, S.; Xu, X. A New Solid Polymer Electrolyte Incorporating $Li_{10}GeP_2S_{12}$ into a Polyethylene Oxide Matrix for All-Solid-State Lithium Batteries. *J. Power Sources* **2016**, *301*, 47−53.

(21) Li, M.; Kolek, M.; Frerichs, J. E.; Sun, W.; Hou, X.; Hansen, M. R.; Winter, M.; Bieker, P. Investigation of Polymer/Ceramic Composite Solid Electrolyte System: The Case of PEO/LGPS Composite Electrolytes. *ACS Sustainable Chem. Eng.* **2021**, *9* (34), 11314−11322.

(22) Wu, J.; Shen, L.; Zhang, Z.; Liu, G.; Wang, Z.; Zhou, D.; Wan, H.; Xu, X.; Yao, X. All-Solid-State Lithium Batteries with Sulfide Electrolytes and Oxide Cathodes. *Electrochemical Energy Reviews* **2021**, *4* (1), 101−135.

(23) Ruhl, J.; Riegger, L. M.; Ghidiu, M.; Zeier, W. G. Impact of Solvent Treatment of the Superionic Argyrodite Li_6PS_5Cl on Solid-State Battery Performance. *Adv. Energy Sustainability Res.* **2021**, *2*, 2000077.

(24) Tan, D. H.; Banerjee, A.; Deng, Z.; Wu, E. A.; Nguyen, H.; Doux, J. M.; Wang, X.; Cheng, J. H.; Ong, S. P.; Meng, Y. S.; Chen, Z. Enabling Thin and Flexible Solid-State Composite Electrolytes by the Scalable Solution Process. *ACS Applied Energy Materials* **2019**, *2* (9), 6542−6550.

(25) Lee, K.; Kim, S.; Park, J.; Park, S. H.; Coskun, A.; Jung, D. S.; Cho, W.; Choi, J. W. Selection of Binder and Solvent for Solution-Processed All-Solid-State Battery. *J. Electrochem. Soc.* **2017**, *164* (9), A2075.

(26) Su, Y.; Ye, L.; Fitzhugh, W.; Wang, Y.; Gil-González, E.; Kim, I.; Li, X. A More Stable Lithium Anode by Mechanical Constriction for Solid State Batteries. *Energy Environ. Sci.* **2020**, *13* (3), 908−916.

(27) Miura, A.; Rosero-Navarro, N. C.; Sakuda, A.; Tadanaga, K.; Phuc, N. H.; Matsuda, A.; Machida, N.; Hayashi, A.; Tatsumisago, M. Liquid-Phase Syntheses of Sulfide Electrolytes for All-Solid-State Lithium Battery. *Nature Reviews Chemistry* **2019**, *3* (3), 189−198.

(28) Liang, J.; Chen, N.; Li, X.; Li, X.; Adair, K. R.; Li, J.; Wang, C.; Yu, C.; Norouzi Banis, M.; Zhang, L.; et al. $Li_{10}Ge(P_{1-x}Sb_x)_2S_{12}$ Lithium-Ion Conductors with Enhanced Atmospheric Stability. *Chem. Mater.* **2020**, *32* (6), 2664−2672.

(29) Xu, F.; Deng, S.; Guo, Q.; Zhou, D.; Yao, X. Quasi-Ionic Liquid Enabling Single-Phase Poly(vinylidene fluoride)-Based Polymer Electrolytes for Solid-State $LiNi_{0.6}Co_{0.2}Mn_{0.2}O_2$|| Li Batteries with Rigid-Flexible Coupling Interphase. *Small Methods* **2021**, *5* (7), 2100262.

(30) Zhang, Y.; Chen, R.; Wang, S.; Liu, T.; Xu, B.; Zhang, X.; Wang, X.; Shen, Y.; Lin, Y.-H.; Li, M.; et al. Free-Standing Sulfide/Polymer Composite Solid Electrolyte Membranes with High Conductance for All-Solid-State Lithium Batteries. *Energy Storage Mater.* **2020**, *25*, 145−153.
(31) Li, Y.; Arnold, W.; Thapa, A.; Jasinski, J. B.; Sumanasekera, G.; Sunkara, M.; Druffel, T.; Wang, H. Stable and Flexible Sulfide Composite Electrolyte for High-Performance Solid-State Lithium Batteries. *ACS Appl. Mater. Interfaces* **2020**, *12* (38), 42653−42659.
(32) Schirmer, R. E. *Modern Methods of Pharmaceutical Analysis*; CRC Press, 1990.
(33) Yamamoto, M.; Terauchi, Y.; Sakuda, A.; Takahashi, M. Binder-Free Sheet-Type All-Solid-State Batteries with Enhanced Rate Capabilities and High Energy Densities. *Sci. Rep.* **2018**, *8* (1), 1212.
(34) Fitzhugh, W.; Wu, F.; Ye, L.; Su, H.; Li, X. Strain-Stabilized Ceramic-Sulfide Electrolytes. *Small* **2019**, *15* (33), 1901470.
(35) Wang, Z. Q.; Wu, M. S.; Liu, G.; Lei, X. L.; Xu, B.; Ouyang, C. Y. Elastic Properties of New Solid State Electrolyte Material $Li_{10}GeP_2S_{12}$: A Study from First-Principles Calculations. *Int. J. Electrochem. Sci.* **2014**, *9* (2), 562−568.
(36) Wang, Y.; Ye, L.; Chen, X.; Li, X. A Two-Parameter Space to Tune Solid Electrolytes for Lithium Dendrite Constriction. *JACS Au* **2022**, *2* (4), 886−897.
(37) Chivers, T.; Elder, P. J. Ubiquitous Trisulfur Radical Anion: Fundamentals and Applications in Materials Science, Electrochemistry, Analytical Chemistry and Geochemistry. *Chem. Soc. Rev.* **2013**, *42* (14), 5996−6005.
(38) Steudel, R.; Chivers, T. The Role of Polysulfide Dianions and Radical Anions in the Chemical, Physical and Biological Sciences, Including Sulfur-Based Batteries. *Chem. Soc. Rev.* **2019**, *48* (12), 3279−3319.
(39) Ye, L.; Gil-González, E.; Li, X. $Li_{9.54}Si_{1.74}(P_{1-x}Sb_x)_{1.44}S_{11.7}Cl_{0.3}$: A Functionally Stable Sulfide Solid Electrolyte in Air for Solid-State Batteries. *Electrochem. Commun.* **2021**, *128*, 107058.
(40) Tan, D. H.; Banerjee, A.; Chen, Z.; Meng, Y. S. From Nanoscale Interface Characterization to Sustainable Energy Storage Using All-Solid-State Batteries. *Nat. Nanotechnol.* **2020**, *15* (3), 170−180.
(41) Weng, W.; Zhou, D.; Liu, G.; Shen, L.; Li, M.; Chang, X.; Yao, X. Air Exposure towards Stable $Li/Li_{10}GeP_2S_{12}$ Interface for All-Solid-State Lithium Batteries. *Materials Futures* **2022**, *1* (2), 021001.
(42) Lu, P.; Liu, L.; Wang, S.; Xu, J.; Peng, J.; Yan, W.; Wang, Q.; Li, H.; Chen, L.; Wu, F. Superior All-Solid-State Batteries Enabled by a Gas-Phase-Synthesized Sulfide Electrolyte with Ultrahigh Moisture Stability and Ionic Conductivity. *Advanced Material* **2021**, *33*, 2100921.
(43) Pyo, S. H.; Park, J. H.; Chang, T. S.; Hatti-Kaul, R. Dimethyl Carbonate as a Green Chemical. *Curr. Opin. Green Sustainable Chem.* **2017**, *5*, 61−66.
(44) Ye, L.; Fitzhugh, W.; Gil-González, E.; Wang, Y.; Su, Y.; Su, H.; Qiao, T.; Ma, L.; Zhou, H.; Hu, E.; Li, X. Toward Higher Voltage Solid-State Batteries by Metastability and Kinetic Stability Design. *Adv. Energy Mater.* **2020**, *10* (34), 2001569.
(45) Krauskopf, T.; Hartmann, H.; Zeier, W. G.; Janek, J. Toward a Fundamental Understanding of the Lithium Metal Anode in Solid-State Batteries—An Electrochemo-Mechanical Study on the Garnet-Type Solid Electrolyte $Li_{6.25}Al_{0.25}La_3Zr_2O_{12}$. *ACS Appl. Mater. Interfaces* **2019**, *11* (15), 14463−14477.
(46) Peled, E.; Golodnitsky, D.; Ardel, G. Advanced Model for Solid Electrolyte Interphase Electrodes in Liquid and Polymer Electrolytes. *J. Electrochem. Soc.* **1997**, *144* (8), L208.

https://doi.org/10.1021/acsami.2c12920
ACS Appl. Mater. Interfaces XXXX, XXX, XXX−XXX